


# Preclinical Evaluation of the Reversible Monoacylglycerol Lipase PET Tracer (R)-[11C]YH132: Application in Drug Development and Neurodegenerative Diseases

## Journal Article

**Author(s):**

He, Yingfang; Delparente, Aro; Jie, Caitlin V.M.L.; Keller, Claudia; Humm, Roland; Heer, Dominik; Collin, Ludovic; Schibli, Roger; Gobbi, Luca; Grether, Uwe; [Mu, Linjing](#) 

**Publication date:**

2024-04-02

**Permanent link:**

<https://doi.org/https://doi.org/10.3929/ethz-b-000666646>

**Rights / license:**

[Creative Commons Attribution-NonCommercial 4.0 International](#)

**Originally published in:**

ChemBioChem 25(7), <https://doi.org/10.1002/cbic.202300819>

**Funding acknowledgement:**

- Imaging Mitochondrial Dysfunction in Neurodegenerative and Cardiovascular Diseases by Targeting the Alpha Subunit of ATP Synthase (ATP5A) ()

# Preclinical Evaluation of the Reversible Monoacylglycerol Lipase PET Tracer (R)-[<sup>11</sup>C]YH132: Application in Drug Development and Neurodegenerative Diseases

Yingfang He,<sup>[a, c]</sup> Aro Delparente,<sup>[a]</sup> Caitlin V. M. L. Jie,<sup>[a]</sup> Claudia Keller,<sup>[a]</sup> Roland Humm,<sup>[b]</sup> Dominik Heer,<sup>[b]</sup> Ludovic Collin,<sup>[b]</sup> Roger Schibli,<sup>[a]</sup> Luca Gobbi,<sup>[b]</sup> Uwe Grether,<sup>[b]</sup> and Linjing Mu<sup>\*[a]</sup>

Monoacylglycerol lipase (MAGL) plays a crucial role in the degradation of 2-arachidonoylglycerol (2-AG), one of the major endocannabinoids in the brain. Inhibiting MAGL could lead to increased levels of 2-AG, which showed beneficial effects on pain management, anxiety, inflammation, and neuroprotection. In the current study, we report the characterization of an enantiomerically pure (R)-[<sup>11</sup>C]YH132 as a novel MAGL PET tracer. It demonstrates an improved pharmacokinetic profile compared to its racemate. High *in vitro* MAGL specificity of (R)-[<sup>11</sup>C]YH132 was confirmed by autoradiography studies using

mouse and rat brain sections. *In vivo*, (R)-[<sup>11</sup>C]YH132 displayed a high brain penetration, and high specificity and selectivity toward MAGL by dynamic PET imaging using MAGL knockout and wild-type mice. Pretreatment with a MAGL drug candidate revealed a dose-dependent reduction of (R)-[<sup>11</sup>C]YH132 accumulation in WT mouse brains. This result validates its utility as a PET probe to assist drug development. Moreover, its potential application in neurodegenerative diseases was explored by *in vitro* autoradiography using brain sections from animal models of Alzheimer's disease and Parkinson's disease.

## Introduction

The endocannabinoid system (ECS) is a sophisticated network activated by endogenous signaling lipids such as 2-arachidonoylglycerol (2-AG) and anandamide (AEA). In reaction to neural activity, endocannabinoids 2-AG and AEA are synthesized 'on-demand' in response to various physiological signals, serving as retrograde messengers that regulate the release of neurotransmitters. The ECS is a complex cell signaling system that involves diverse physiological processes within the central nervous system (CNS), including brain plasticity, learning and memory, neuronal development, cellular fate, nociception, and inflammation.<sup>[1,2]</sup> Monoacylglycerol lipase (MAGL) is a membrane-bound soluble hydrolase localized in the axon terminal and is recognized as a predominant guardian in endocannabinoid signaling. MAGL degrades 85% of brain 2-AG into glycerol

and arachidonic acid, a major arachidonate precursor pool for neuroinflammatory prostaglandins.<sup>[3,4]</sup> Increasing evidence suggests that MAGL inhibition provides beneficial effects on pain management, anxiety, inflammation, and neuroprotection.<sup>[5]</sup>

Chronic, uncontrolled and persistent inflammation has been recognized as a contributor to neurodegenerative diseases, including Alzheimer's disease (AD) and Parkinson's disease (PD).<sup>[6,7]</sup> Due to the essential role of MAGL in prostanoid receptor signaling,<sup>[8]</sup> pharmacological inhibition of MAGL has been considered as a potential strategy for combating neurodegeneration.<sup>[9]</sup> In pre-clinical studies, selective and potent MAGL inhibitors have demonstrated neuroprotective effects and the ability to suppress inflammation.<sup>[10]</sup> For example, JZL184, an early-developed irreversible MAGL inhibitor, demonstrated attenuation of cortical and hippocampal  $\beta$ -amyloid aggregation in the 5xFAD transgenic mouse model of AD,<sup>[11]</sup> and prevent dopaminergic neuronal loss in a 1-methyl-4-phenyl-1,2,3,6-tetrahydropyridine (MPTP) induced mouse model of PD.<sup>[12]</sup> Very recently, elevated MAGL expression was found in the brain of AD mouse models and in human AD patient post-mortem hippocampal tissues by western blot and immunohistochemistry.<sup>[13]</sup> Nevertheless, further investigation into MAGL expression levels in AD and PD is still limited.

Apart from the above-mentioned bioanalytic methods, positron emission tomography (PET) has been increasingly recognized as an irreplaceable imaging modality in neuroscience.<sup>[14]</sup> PET is a non-invasive imaging technique that plays a crucial role in supporting drug development. It can facilitate the quantitative measurement of target engagement for drug candidates as well as support the determination of optimal drug dosage. PET studies using an appropriate molecular probe enable the assessment of target expression

[a] Y. He, A. Delparente, C. V. M. L. Jie, C. Keller, R. Schibli, L. Mu  
Institute of Pharmaceutical Sciences, ETH Zurich, Vladimir-Prelog-Weg 4,  
CH-8093 Zurich, Switzerland  
E-mail: linjing.mu@pharma.ethz.ch

[b] R. Humm, D. Heer, L. Collin, L. Gobbi, U. Grether  
Pharma Research and Early Development, Roche Innovation Center Basel, F.  
Hoffmann-La Roche Ltd, CH-4070 Basel, Switzerland

[c] Y. He  
Present address: Institute of Radiation Medicine, Fudan University, Xietu  
Road 2094, Shanghai 200032, China

Supporting information for this article is available on the WWW under  
<https://doi.org/10.1002/cbic.202300819>

© 2024 The Authors. ChemBioChem published by Wiley-VCH GmbH. This is an open access article under the terms of the Creative Commons Attribution Non-Commercial License, which permits use, distribution and reproduction in any medium, provided the original work is properly cited and is not used for commercial purposes.

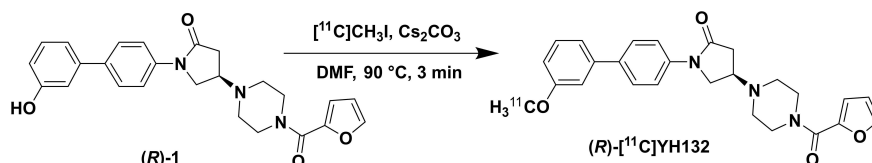
levels under both physiological and pathological conditions. For instance, longitudinal PET studies using [ $^{11}\text{C}$ ]ABP688 revealed a significant reduction of binding to metabotropic glutamate receptor 5 (mGluR5) in a Huntington disease animal model which suggested that mGluR5 PET could be used to monitor the progression of Huntington disease.<sup>[15]</sup> In our previous studies of developing reversible MAGL PET tracers, racemic compound *rac*-YH132 revealed a proper lipophilicity ( $\log D_{7.4} = 2.24 \pm 0.15$ ) and a high MAGL inhibition potency (9 nM).<sup>[16]</sup> Given the fact that the *R*-isomer of the 4-(piperazin-1-yl)-pyrrolidin-2-one derivative is more potent than its *S*-isomer towards MAGL inhibition, this current study focuses on the characterization of the enantiomerically pure (*R*)-[ $^{11}\text{C}$ ]YH132 as a MAGL PET tracer.

Herein, we disclose the chiral separation of *rac*-YH132, radiosynthesis of (*R*)-[ $^{11}\text{C}$ ]YH132 and its *in vitro* and *in vivo* evaluation. Autoradiography using brain sections from rodents and PET imaging with MAGL knockout (KO) and wild-type (WT) mice were performed for evaluating the specificity and selectivity of (*R*)-[ $^{11}\text{C}$ ]YH132 towards MAGL. After confirming the *in vitro* and *in vivo* specific binding of (*R*)-[ $^{11}\text{C}$ ]YH132, blocking studies were conducted using different doses of MAGLi 432 (0.008 and 0.045 mg/kg), a potent and selective MAGL inhibitor developed by Roche.<sup>[17]</sup> Moreover, brain sections from AD/PD transgenic mouse models were screened via *in vitro* autoradiography to understand whether (*R*)-[ $^{11}\text{C}$ ]YH132 could identify altered MAGL expression levels in the diseased brains compared to their respective controls. Hematoxylin & Eosin (H&E) staining was conducted using brain sections after *in vitro* autoradiography to provide histological information of the samples. Our initial findings provide evidence that MAGL could serve not only as a valuable drug target but also as a potential biomarker for monitoring disease progression.

## Results

### Chiral separation

*rac*-YH132 and its phenolic precursor (**1**) were synthesized as previously reported.<sup>[16]</sup> The chiral separation was achieved by supercritical fluid chromatography. The enantiomeric excess (ee) was tested by high-performance liquid chromatography (HPLC)-mass spectrometry (MS) using a chiral column. The ee values were determined as 100% and 98% for (*R*)-YH132 and its hydroxyl precursor ((*R*)-**1**), respectively. The corresponding chromatograms are shown in the supporting information (Figure S1).



**Scheme 1.** Radiosynthesis of (*R*)-[ $^{11}\text{C}$ ]YH132.

### Measurement of inhibition constants

The half-maximal inhibitory concentration (IC<sub>50</sub>) of (*R*)-YH132 was measured in duplicate using an enzymatic assay. The compound possesses IC<sub>50</sub> values of 6.5 nM and 4.3 nM for human and mouse MAGL, respectively. As expected, (*R*)-YH132 exhibited more potent MAGL inhibition than its racemic form *rac*-YH132 in mouse (4.3 nM vs. 9.0 nM). This result is in agreement with the previous findings of the stereochemistry influence on MAGL inhibition from different research groups.<sup>[16,18]</sup>

### Radiosynthesis of (*R*)-[ $^{11}\text{C}$ ]YH132

(*R*)-[ $^{11}\text{C}$ ]YH132 was obtained via a single-step *O*-methylation of the phenolic precursor ((*R*)-**1**) with [ $^{11}\text{C}$ ]CH<sub>3</sub>I in the presence of Cs<sub>2</sub>CO<sub>3</sub> (Scheme 1). The total synthesis time including radio-labeling and semi-HPLC purification was around 40 min. Radiochemical purity of the final product was greater than 99%. The molar activity of the tracer was between 478 and 1738 GBq/ $\mu\text{mol}$  at the end of radiosynthesis ( $n=10$ ). The identity of (*R*)-[ $^{11}\text{C}$ ]YH132 was confirmed by co-injection with the non-radioactive (*R*)-YH132.

### *In vitro* plasma stability and autoradiography

The plasma stability of (*R*)-[ $^{11}\text{C}$ ]YH132 was evaluated by co-incubation with human, rat or mouse plasma. In all cases, the radiochemical purity of (*R*)-[ $^{11}\text{C}$ ]YH132 was above 99% after 40 min incubation at physiological temperature of 37 °C. The radio-UPLC chromatograms are shown in the supporting information (Figure S2).

Incubation of (*R*)-[ $^{11}\text{C}$ ]YH132 (~1 nM) with mouse or rat brain sections revealed a heterogeneous distribution of radioactive accumulation, which aligns with the MAGL expression pattern in rodents.<sup>[19,22]</sup> As shown in Figure 1, high radioactivity accumulation of (*R*)-[ $^{11}\text{C}$ ]YH132 was observed in the cortex, hippocampus and striatum in rat brain sections under baseline conditions. In blocking studies, two irreversible and potent MAGL inhibitors, SAR127303 and PF-06809247,<sup>[20,21]</sup> were used to compete with (*R*)-[ $^{11}\text{C}$ ]YH132 for specific binding to MAGL. A substantial reduction and homogenous distribution of radioactivity were observed in both cases indicating the *in vitro* specificity of the novel tracer. Further studies using MAGL KO and WT mouse brain sections revealed high selectivity of (*R*)-[ $^{11}\text{C}$ ]YH132 as the high radioactive signal in MAGL-rich brain

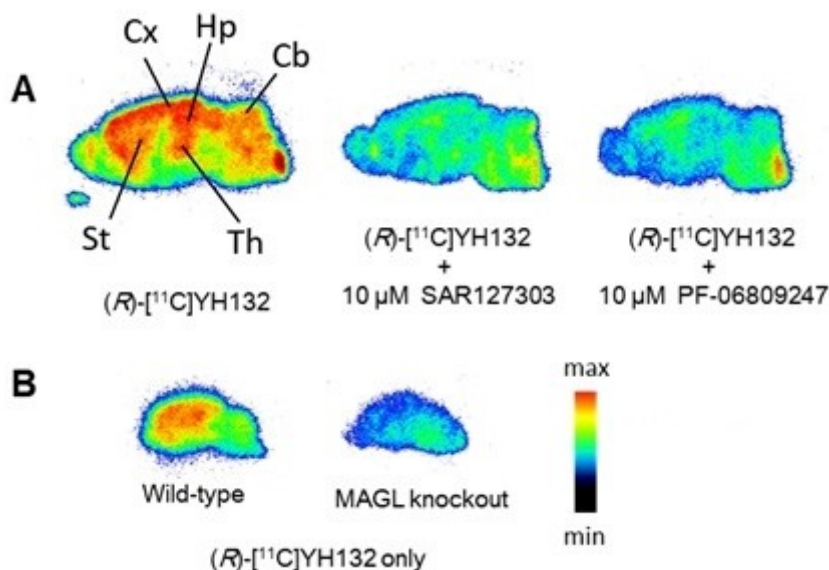


**Figure 1.** *In vitro* autoradiograms of (*R*)-[<sup>11</sup>C]YH132 (Cx=cortex; Hp=hippocampus; Cb=cerebellum; St=striatum; Th=thalamus) in rat (A) and mouse (B) brain sections.

regions of WT mouse was abolished in that of MAGL KO brain sections.

#### Free fractions of (*R*)-[<sup>11</sup>C]YH132 in human and mouse plasma

The free fractions of (*R*)-[<sup>11</sup>C]YH132 in mouse and human plasma were determined as  $23 \pm 1\%$  ( $n=3$ ) and  $19 \pm 1\%$  ( $n=3$ ), respectively. The high plasma free fraction of (*R*)-[<sup>11</sup>C]YH132 ( $> 15\%$ ) suggests a substantial availability of the radioactive probe in the bloodstream, facilitating its ability to cross the blood-brain barrier as well as a reduced risk of nonspecific binding *in vivo*.<sup>[23,24]</sup>

#### *In vivo* PET imaging

Further evaluation of (*R*)-[<sup>11</sup>C]YH132 was performed via *in vivo* PET/CT imaging to compare it with *rac*-[<sup>11</sup>C]YH132 in MAGL KO and WT mice. The time activity curves (TACs) of (*R*)-[<sup>11</sup>C]YH132 and *rac*-[<sup>11</sup>C]YH132 are depicted in Figure 2A. Compared to *rac*-[<sup>11</sup>C]YH132, higher specific signals were achieved with (*R*)-[<sup>11</sup>C]YH132. The maximal accumulation of (*R*)-[<sup>11</sup>C]YH132 was reached within 5 min post-injection (p.i.) with standardized uptake value (SUV) of  $1.33 \pm 0.18$  (average  $\pm$  SD,  $n=4$ ) in WT mice brains. Significant washout (ratio of  $SUV_{5\text{min}}/SUV_{60\text{min}} = 1.33/0.65$ ) was observed in the late time period of PET imaging, suggesting a reversible binding of (*R*)-[<sup>11</sup>C]YH132 *in vivo*. In MAGL KO mice brains, remarkably reduced radioactivity was observed compared to that of WT mice indicating high specific binding of (*R*)-[<sup>11</sup>C]YH132 towards MAGL. The PET images averaged from 9.0 to 60 min p.i. are displayed in Figure 2B. High radioactivity uptake was evident in the cortex, striatum and hippocampus, which corroborates the *in vitro* autoradiograms of (*R*)-[<sup>11</sup>C]YH132. The TACs of (*R*)-[<sup>11</sup>C]YH132 in various

brain regions, including striatum, hippocampus, cortex, thalamus and cerebellum are presented in the supporting information (Figure S3).

#### Effect of MAGLi 432 on mice brain uptake of (*R*)-[<sup>11</sup>C]YH132

Blocking studies with MAGLi 432, a potent and selective reversible MAGL inhibitor regulating MAGL activity in neurovasculature, demonstrated a reduction in (*R*)-[<sup>11</sup>C]YH132 accumulation in mouse brains (Figure 3A). Pretreatment with either 0.008 mg/kg or 0.045 mg/kg MAGLi 432 decreased the whole brain uptake of the radiotracer in a dose-dependent manner. The area under the curve (AUC) was calculated from TACs in different brain regions as presented in Figure 3B. In high MAGL expressing regions (i.e. cortex, striatum and hippocampus) a clear dose-dependency was observed. Whereas a weaker dose-dependent effect was seen in the low MAGL expressing regions (hypothalamus and brainstem).<sup>[19]</sup>

#### *In vitro* autoradiography and H&E staining on brain sections of diseased animal models

To explore the potential application of (*R*)-[<sup>11</sup>C]YH132 in neurodegenerative diseases, *in vitro* autoradiography studies were performed using brain sections of AD and PD animal models (Figure 4A and 4B). In both cases, semiquantification of the cortex region was performed for statistical evaluation. The densities of radioactive signals are depicted in Figure 4C and D with further details provided in the supporting information (Figure S4–5 and Table S1–2). In addition, the brain tissues were stained with hematoxylin and eosin (H&E) to provide the corresponding morphological information. Brain tissues from Tau-P301 L mutant mice demonstrated similar distribution of

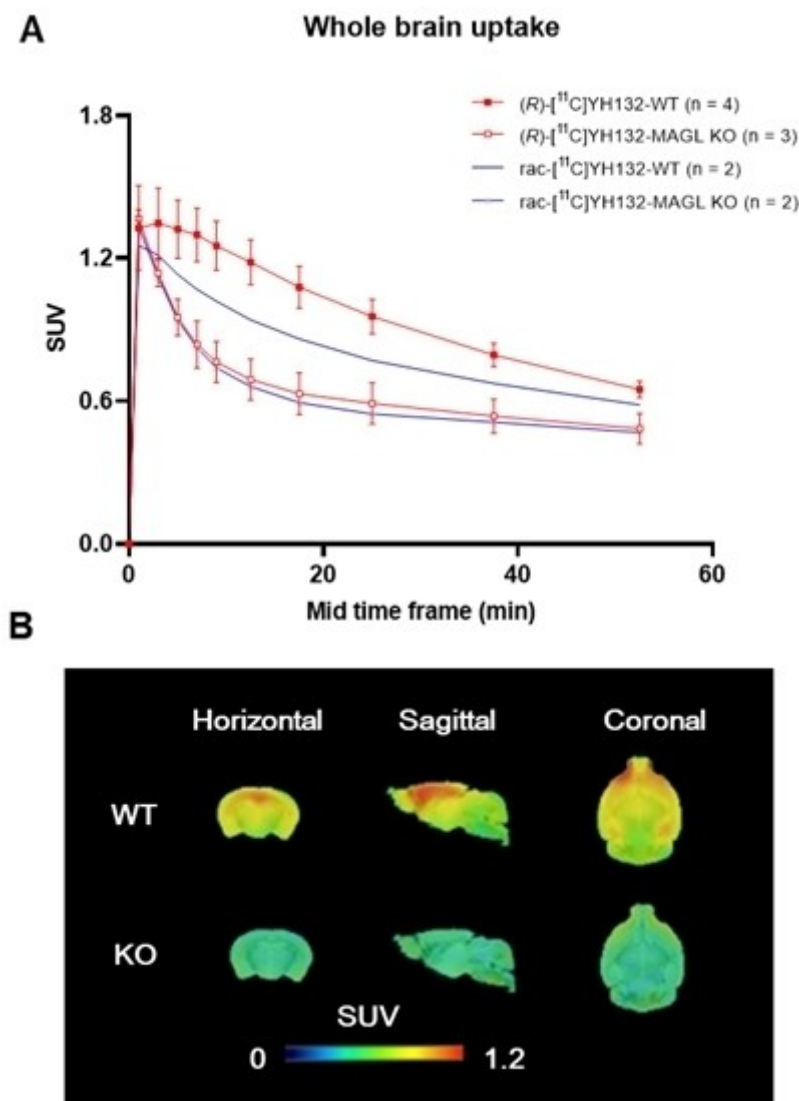


**Figure 2.** (A) Time activity curves (TACs) of (R)-[<sup>11</sup>C]YH132 and rac-[<sup>11</sup>C]YH132 in the whole brain. The data of rac-[<sup>11</sup>C]YH132 was published by He *et al.*<sup>[16]</sup> (B) The representative PET images of (R)-[<sup>11</sup>C]YH132 in MAGL KO and WT mouse brains averaged from 9.0 to 60 min.

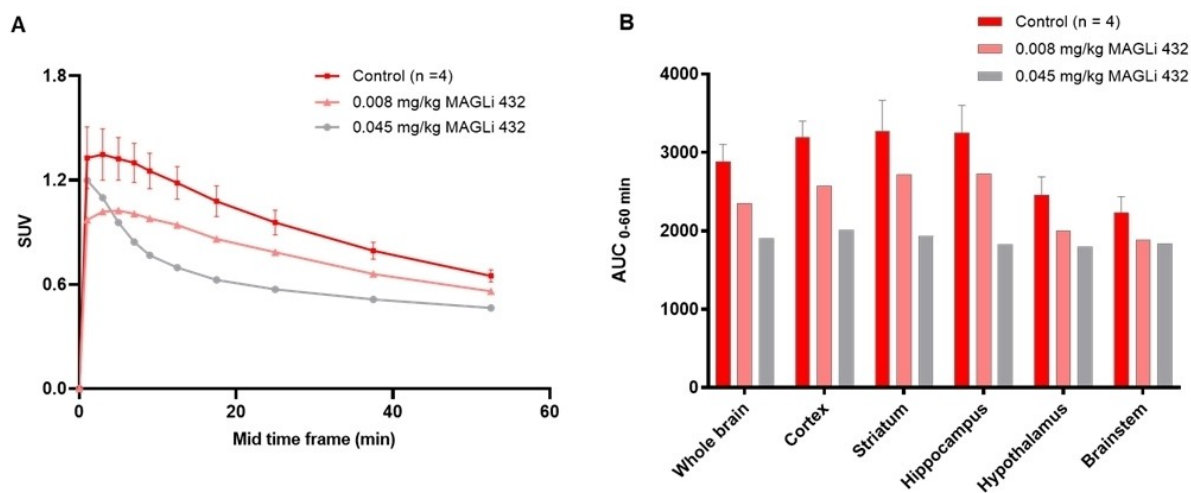


**Figure 3.** (A) TACs of (R)-[<sup>11</sup>C]YH132 in the whole brain under control and blocking conditions; (B) AUCs calculated from TACs in different brain regions.

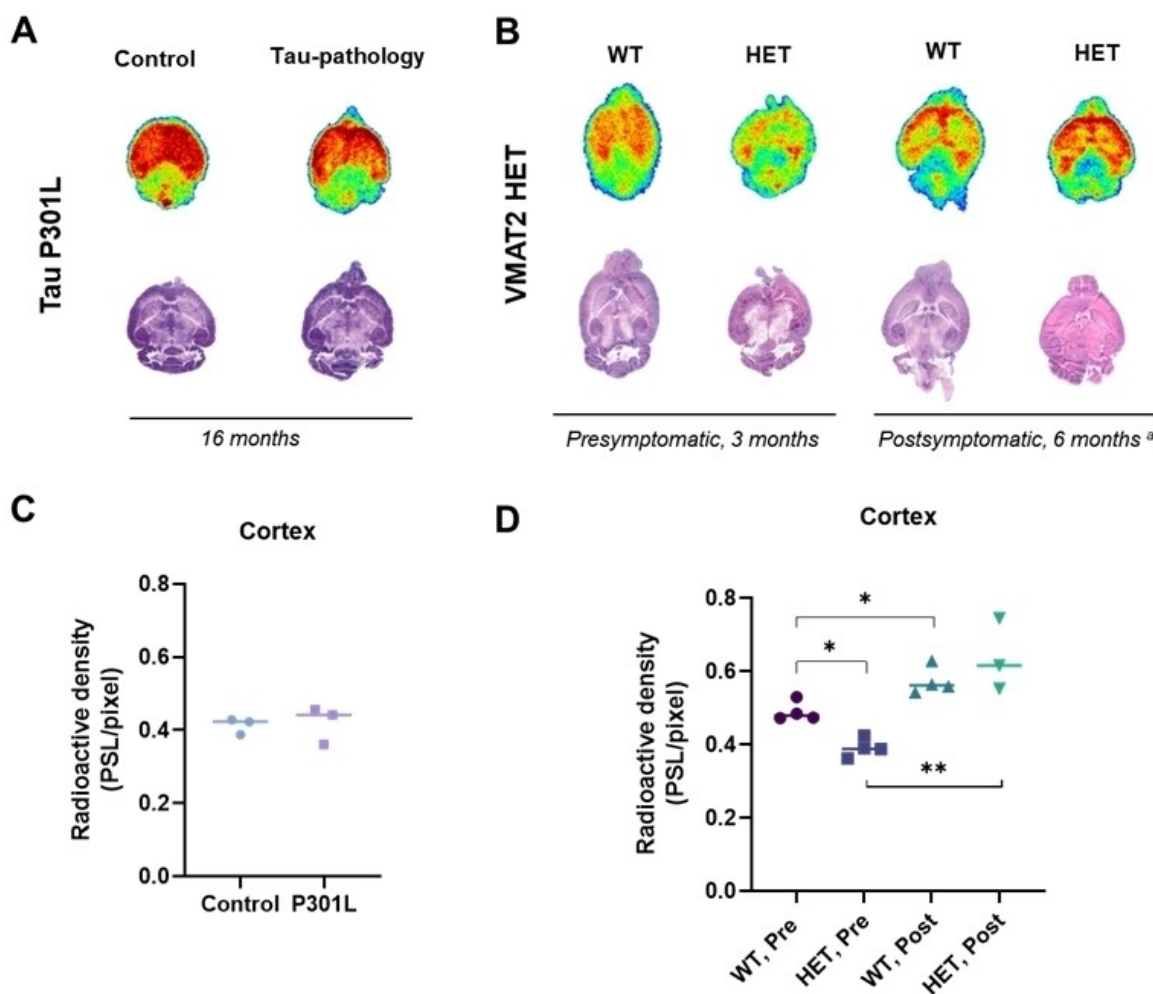


**Figure 4.** (A) Representative autoradiograms of  $(R)$ - $[^{11}\text{C}]\text{YH132}$  from Tau P301 L mouse brain sections and their H&E staining results. (B) The representative autoradiograms of  $(R)$ - $[^{11}\text{C}]\text{YH132}$  from VMAT2 HET mouse brain section and their H&E staining results. (C) Semiquantification of  $(R)$ - $[^{11}\text{C}]\text{YH132}$  in cortex region from Tau P301 L. (D) Semiquantification in cortex region from VMAT2 HET. <sup>a</sup> H&E-stained image of the VMAT2 HET mouse brain section was from brain tissue nearby rather than the sections used in autoradiography. \* $p < 0.05$ , \*\* $p < 0.005$ .

radioactive signals to those of the WT brain sections. This observation was confirmed by semiquantification of the radioactive signals in the cortex area, where no significant difference was determined (Figure 4C). The radioactivity density of  $(R)$ - $[^{11}\text{C}]\text{YH132}$  in vesicular monoamine transporter 2 (VMAT2) heterozygous (HET) mouse brain sections, as well as from its corresponding WT, profoundly increased over time suggesting an age-dependent MAGL expression in mouse (Figure 4D). Notably, significantly lower radioactive accumulation was found in the cortex of the pre-symptomatic VMAT2 HET mouse in comparison with the WT mouse ( $-20\%$ ,  $p < 0.005$ ) whilst, on average, higher radioactive density of  $(R)$ - $[^{11}\text{C}]\text{YH132}$  was found in post-symptomatic stage of the VMAT2 HET brain sections.

## Discussion

ETH Zurich and F. Hoffmann-La Roche Ltd collaborated over the last decade for the development of innovative PET tracers for imaging various targets in the endocannabinoid system. It is a

fruitful collaboration covering multiple disciplines, such as drug discovery, lead optimization, preclinical evaluation and clinic translation. So far, we have successfully developed  $[^{18}\text{F}]\text{RoSMA-18-d}_6$  for imaging cannabinoid type 2 receptors.<sup>[25,26]</sup> This radiotracer was recently selected for a first-in-human trial to investigate its regional distribution in the brain and spinal cord for assessing CB2 expression in healthy volunteers and patients with Amyotrophic Lateral Sclerosis (ClinicalTrials.gov NCT05880563). For the ongoing MAGL project, we have synthesized and investigated  $[^{11}\text{C}]\text{RO7284390}$  based on Roche's morpholin-3-one derivatives library and  $[^{18}\text{F}]\text{YH149}$  based on the pyrrolidin-2-one lead structure from the literature.<sup>[16,27,28]</sup> During the collaboration, we recognized that a good drug candidate may not necessarily lead to a suitable candidate for PET imaging. The pursued features of comparatively slow pharmacokinetics and long target occupancy for a drug candidate are not favorable for a PET tracer due to the inability or lengthy time it takes to reach an equilibrium stage in a practical PET study, as exemplified with  $[^{11}\text{C}]\text{RO7279991}$  and  $[^{11}\text{C}]\text{RO7284390}$ .<sup>[27,28]</sup> On the other hand,  $[^{18}\text{F}]\text{YH149}$ , with high

brain penetration and reversibility, holds great potential to support drug development. Whilst the use of fluorine-18 in radioligands is advantageous due to its low positron energy and relatively long half-life (109.8 min), a carbon-11 labeled radiotracer with short physical half-life (20.4 min) provides additional opportunities in the study design. This is particularly beneficial for time course occupancy studies in which subjects can be scanned under baseline and several time points post pharmacological intervention without causing high radioactivity burden. It enables investigation into the correlation between drug plasma concentration and target occupancy in a relatively short time period and small cohort.<sup>[29]</sup> Thus, in the current study, we focused on the development of a reversible MAGL PET tracer labeled with carbon-11.

Radiotracer (*R*)-[<sup>11</sup>C]YH132 was synthesized *via* one-step *O*-methylation approach, which afforded a high molar activity appropriate for neuroimaging. The *in vitro* autoradiography of (*R*)-[<sup>11</sup>C]YH132 revealed a heterogeneous distribution in rodent brains. The low and homogeneous radioactivity distribution on MAGL KO brain sections confirmed low levels of binding to non-target proteins and cell membranes. Dynamic PET imaging with (*R*)-[<sup>11</sup>C]YH132 exhibited high brain permeability in WT mice with maximal SUV values of  $1.33 \pm 0.18$  ( $n=4$ ) at 1 min post-injection, which is comparable with [<sup>18</sup>F]YH149 ( $1.63 \pm 0.27$  at 1 min p.i.,  $n=4$ ).<sup>[16]</sup> In Figure 2A, (*R*)-[<sup>11</sup>C]YH132 accomplished a significantly higher AUC in WT mice brains than *rac*-[<sup>11</sup>C]YH132. This difference is likely contributed by the increased inhibition potency of the *R* enantiomer of YH132 towards mouse MAGL ( $IC_{50}=4.3$  nM vs.  $IC_{50}=9.0$  nM for *rac*-YH132).<sup>[16]</sup> While the signals remaining in MAGL KO brain indicate a moderate levels of non-specific binding for both tracers.

MAGL-mediated production of 2-AG enhances the local concentration of arachidonic acid and consequently leads to neuroinflammation which is involved in several neurodegenerative diseases. A reversible inhibitor developed for the modulation of MAGL activity, MAGLi 432, was employed to investigate the utility of (*R*)-[<sup>11</sup>C]YH132 in MAGL drug development. A dose-dependent reduction of the radioactive accumulation in the mouse brains was observed by injection a 0.008 or 0.045 mg/kg dose of MAGLi 432 prior to (*R*)-[<sup>11</sup>C]YH132 administration. These results demonstrated the capacity of (*R*)-[<sup>11</sup>C]YH132 to investigate the drug-target engagement and to determine optimal drug dosage by target occupancy studies. To explore the potential use of (*R*)-[<sup>11</sup>C]YH132 as a biomarker for monitoring disease progression, *in vitro* autoradiography was carried out using AD and PD mouse brain sections. Semi-quantification of the radioactive signals did not show significant differences in the cortical region from 16-month mutant Tau-P301 L mouse. However, previous studies by Wang *et al* reported an elevated MAGL expression in the hippocampal extractions of 9-month 3×Tg-AD mice, an animal model containing three mutations associated with familial AD (APP, MAPT P301 L and PSEN1 M146 V).<sup>[13]</sup> Further investigation using the same AD model is planned in future studies. To evaluate potential use in PD, brain sections of VMAT2 HET mice – a PD mouse model that is vulnerable to MPTP toxicity and displays PD-like motor deficit<sup>[30–32]</sup> – was investigated. In comparison to

WT mice brains, a significant reduction of MAGL-specific radioactive accumulation was found in VMAT2 HET mice brains at pre-symptomatic stage. Moreover, the specific accumulation of (*R*)-[<sup>11</sup>C]YH132 in the cortex was increased by 1.6-fold from pre-symptomatic to post-symptomatic stage ( $p < 0.005$ ). This suggests that there may be an association between MAGL and disease progression in the VMAT2 HET mouse model. A longitudinal PET together with western blotting and behavioural experiments, such as gait recognition and fingerprint analysis, is of high interest to explore whether (*R*)-[<sup>11</sup>C]YH132 could serve as an imaging biomarker for monitoring disease progression in VMAT2 HET mice.

## Conclusions

In conclusion, we have successfully developed and characterized (*R*)-[<sup>11</sup>C]YH132 as a novel PET tracer for imaging MAGL in mice brain. It exhibits high MAGL inhibition potency *in vitro*, high MAGL specificity and selectivity *in vivo*. Its reversible kinetics enable it as a MAGL PET tracer to support CNS MAGL drug development, especially in assessing drug target engagement and determining the optimal dose via drug occupancy studies. Our preliminary *in vitro* autoradiography results using diseased mouse brain sections indicate that, in addition to accelerating drug discovery and monitoring therapeutic interventions, MAGL imaging may be of interest for disease staging in a PD animal model. Further investigation is warranted to fully understand the role of MAGL during disease progression and explore its potential as a biomarker for neurodegenerative diseases.

## Materials and methods

All chemicals, unless further stated, were purchased from commercially available suppliers (Fluorochem Ltd, Sigma-Aldrich, Apollo Scientific Ltd or Alfa Aesar) and used directly. Radiolabeled compounds were purified with semi-preparative high performance liquid chromatography (HPLC) system using ACE 5C18-300 column (250×10 mm) with 0.1% H<sub>3</sub>PO<sub>4</sub> in water as mobile phase A and MeCN as mobile phase B. Gradient method with 0.0–6.0 min, 5–30% B; 6.0–8.0 min, 30–40% B; 8.0–12.0 min, 40–50% B; 12.0–18.0 min, 50–95% B; 18.0–20.0 min, 95% B was applied at a flow of 4 mL/min and a wavelength of 254 nm. The radioactive products were analyzed with an Agilent 1100 series HPLC system, equipped with UV detector and a GabiStar radiodetector (Raytest) using an ACE XDB-C18 Zorbax column (75 mm×4.6 mm, 3.5 μm) with the following condition: 0.0–3.0 min, 5–30% B; 3.0–4.0 min, 30–40% B; 4.0–6.0 min, 40–50% B; 6.0–9.0 min, 50–95% B; 9.0–10.0 min, 95% B with a flow of 1 mL/min at 254 nm. The identity of the radiotracer was confirmed by co-injection with the non-radio-labeled reference compound. The plasma stability was analyzed by radio-ultraperformance liquid chromatography (UPLC, Waters) equipped with ACQUITY UPLC BEH C18 Column (130 Å, 1.7 μm, 2.1 mm×50 mm) using 10 mM NH<sub>4</sub>HCO<sub>3</sub> and MeCN as

the eluents. A gradient method (0.0–2.0 min, 5–30% MeCN; 2.0–3.5 min, 30–50% MeCN; 3.5–4.0 min, 50–90% MeCN; 4.0–6.0 min, 90% MeCN) was employed with a flow of 0.6 mL/min.

Animal studies were performed in compliance with the Swiss animal protection and welfare legislation, and were approved by the Veterinary Office of Canton Zurich (ZH 28/2018). MAGL knockout (KO) and corresponding wild-type (WT) mice were from Taconic Biosciences (Silkeborg, Denmark). The animal care was conducted under standard conditions. The brain sections of vesicular monoamine transporter 2 (VMAT2) heterozygous (HET) and Tau P301 L mutant mice were kindly provided by Dr. Daniela Noain (University Hospital Zurich) and Prof. Dr. Jan Klohs (University of Zurich and ETH Zurich).

### Chiral separation

Chiral separation was carried out using supercritical fluid chromatography (SFC) on a Shimadzu system equipped with LC-40 SF solvent delivery module, DGU403 degassing unit SPD M40 photo diode array detector, HEX-40 solvent heat exchanger, LC-20AR liquid chromatograph, LC-20AP preparative liquid chromatograph, SFC-40P back pressure regulator, CTO-40 C column oven and a ChiralPak IH, 5  $\mu$ m, 250x20 mm column.

(*R*)-YH132: SFC mobile phase 45% MeOH in CO<sub>2</sub>; <sup>1</sup>H NMR (300 MHz, chloroform-*d*):  $\delta$  7.68–7.64 (m, 2H), 7.62–7.57 (m, 2H), 7.48 (dd, *J* = 1.8, 0.8 Hz, 1H), 7.38–7.33 (m, 1H), 7.18–7.15 (m, 1H), 7.11–7.10 (m, 1H), 7.03 (dd, *J* = 3.4, 0.8 Hz, 1H), 6.91–6.87 (m, 1H), 6.49 (dd, *J* = 3.4, 1.8 Hz, 1H), 4.00 (dd, *J* = 9.5, 7.4 Hz, 1H), 3.92–3.81 (m, 2H), 3.87 (s, 3H), 3.35–3.25 (m, 4H), 2.84–2.58 (m, 6H). LC-MS (ESI) *m/z* = 446.3 ([*M* + H]<sup>+</sup>).

(*R*)-1.: SFC mobile phase 40% MeOH in CO<sub>2</sub>; <sup>1</sup>H NMR (300 MHz, chloroform-*d*):  $\delta$  7.69–7.64 (m, 2H), 7.61–7.57 (m, 2H), 7.48 (dd, *J* = 1.8, 0.8 Hz, 1H), 7.30 (dd, *J* = 7.7, 7.7 Hz, 1H), 7.15–7.12 (m, 1H), 7.10–7.09 (m, 1H), 7.03 (dd, *J* = 3.4, 0.8 Hz, 1H), 6.82 (ddd, *J* = 8.0, 2.6, 0.9 Hz, 1H), 6.49 (dd, *J* = 3.5, 1.7 Hz, 1H), 5.59 (br s, 1H), 4.99 (dd, *J* = 9.5, 7.4 Hz, 1H), 3.92–3.81 (m, 4H), 3.49 (d, *J* = 5.4 Hz, 1H), 3.35–3.25 (m, 1H), 2.85–2.57 (m, 6H). LC-MS (ESI) *m/z* = 432.3 ([*M* + H]<sup>+</sup>).

**Measurement of inhibition constants.** The IC<sub>50</sub> value was measured in human and mouse MAGL using the non-labeled compound dissolved in DMSO. The solutions containing *rac*-YH132 or (*R*)-YH132 ranging from 12.5  $\mu$ M to 0.8 pM (0.25  $\mu$ L) were transferred into a 384-well plate. Upon adding 9  $\mu$ L human or mouse MAGL-recombinant assay buffer (50 mM TRIS (GIBCO, 15567-027), 1 mM EDTA (Fluka, 03690), 0.01% Tween 20, v/v and 2.3% DMSO, v/v), the plate was incubated at room temperature for 15 min. Then 2-AG in assay buffer was added to the solution which contains 50 pM MAGL protein, 8  $\mu$ M 2-AG and a concentration range of the tested compound in a total volume of 20  $\mu$ L. After 30 min incubation with gentle shaking at room temperature, the reaction was quenched with 40  $\mu$ L acetonitrile containing 4 pM *d*<sub>8</sub>-arachidonic acid (AA). The mass transitions were determined by an online solid phase extraction system (Agilent Rapidfire) coupled to a triple quadrupole mass spectrometry (Agilent 6460) in ESI<sup>-</sup> mode with *m/z* = 303.1 to 259.1 for AA and *m/z* = 311.1 to 267.0 for *d*<sub>8</sub>-AA, respectively.

The IC<sub>50</sub> values of YH132 was fitted based on the intensity ratio of AA/ *d*<sub>8</sub>-AA under various concentrations.

**Radiosynthesis of (*R*)-[<sup>11</sup>C]YH132.** The synthesis of (*R*)-[<sup>11</sup>C]YH132 was detailed as previously described by our group.<sup>[33]</sup> Briefly, the hydroxyl precursor (*R*)-1 (~0.5 mg) was dissolved in 0.5 mL anhydrous DMF with 5 mg Cs<sub>2</sub>CO<sub>3</sub>. [<sup>11</sup>C]CH<sub>3</sub>I was produced by reduction of [<sup>11</sup>C]CO<sub>2</sub> (cyclone 18/9 cyclotron, 18 MeV; IBA, Belgium) to [<sup>11</sup>C]CH<sub>4</sub>, followed by iodination to form [<sup>11</sup>C]CH<sub>3</sub>I. [<sup>11</sup>C]CH<sub>3</sub>I was bubbled into the mixture, and the reaction was heated at 90 °C for 3 min. After diluting with 2 mL water, the mixture was loaded to a semi-preparative HPLC for purification. The radioactive fraction with a retention time of 12 min was collected, mixed with 8 mL water, and passed through a C18 light cartridge (Waters, WAT023501). After washing with 5 mL water, the desired product was eluted with 0.5 mL ethanol and diluted with 9.5 mL PBS buffer to give the formulated solution containing around 5% ethanol.

**In vitro plasma stability, autoradiography and hematoxylin-eosin (H&E) staining.** Plasma (300  $\mu$ L) from mouse, rat or human were incubated with (*R*)-[<sup>11</sup>C]YH132 (10  $\mu$ L, 5–10 MBq) at 37 °C for 40 min. An equate volume of ice-cold acetonitrile was added to quench the reaction, and the mixture was briefly vortexed before centrifugation at 5000 rpm for 3 min. The supernatant was passed through a Nalgene syringe filter (0.22  $\mu$ M, PES membrane) and the resulting clear solution was used for UPLC analysis.

Sagittal brain sections from rodents were prepared in the thickness of 10  $\mu$ m with a cryostat (Cryo-Star HM 560 MV; Microm, Thermo Scientific, Wilmington, DE), absorbed on SuperFrost Plus glass slides (Menzel, Braunschweig, Germany), and stored at –20 °C before use. At the day of experiment, slices were firstly thawed on ice for 10 min and pre-conditioned in an HEPES buffer (50 mM HEPES, 1.2 mM MgCl<sub>2</sub>, 110 mM NaCl, 5 mM KCl, 2.5 mM CaCl<sub>2</sub>) containing 3% fatty acid free bovine serum albumin (BSA, Sigma-Aldrich) at 0 °C for 10 min. The slices were left to dry and then incubated with 2–3 nM (*R*)-[<sup>11</sup>C]YH132 at a humidified chamber for 30 min. 10  $\mu$ M SAR127303 or 10  $\mu$ M PF-06809247 were employed particularly on Wistar rat brain slices for blocking. After incubation, the slices were washed once in ice-cold HEPES buffer containing 3% BSA for 2 min, twice in HEPES buffer without BSA for 2 min, and twice with distilled water for 5 s. The slices were attached to the phosphor imager plates (Fuji, Dielsdorf, Switzerland) after drying, and exposure was lasted for 60 min. The films were later scanned by BAS5000 reader (Fuji).

The slides from or closer to *in vitro* autoradiography were placed in a metal rack and immersed in Hematoxylin Gill III (Sigma-Aldrich, GHS332) for 4 min. The rack was then rinsed in tap water until the aqueous solution became clear. After a quick dip in 0.1% HCl solution (~2 seconds), a gentle stream of tap water was enrolled to rinse through the slices (2 mins) for differentiation. The slides were subsequently counterstained with alcoholic-eosin (2 min) and rinsed with tap water. The dehydration was conducted in 100% ethanol (2  $\times$  1 min) followed by immersing in xylene bath (1–2 min) to render the transparency. After performing all the procedures described above, the slides were embedded with a thin layer of quick

hardening mounting medium (Eukitt, Fluka 03989), covered with a glass coverslip, and read on Slide Scanner Panoramic 250 (3D Histech) for image acquisition.

**Free fraction in human and mouse plasma.** The plasma protein binding of (R)-[<sup>11</sup>C]YH132 was measured in triplicate as previously reported.<sup>[34]</sup> 1–2 MBq radiotracer (5–10 μL) was added to 150 μL plasma and incubated at 37°C with gentle shaking for 10 min. The plasma was then transferred to an Amicon centrifugal filter (Millipore, UFC501024) containing 300 μL ice-cold PBS. The mixture was briefly vortexed, and centrifuged at 15000 RCF for 10 min (4°C). The residue was then washed with 100 μL PBS, mixed with pipette and centrifuged again. After repeating this step for three times, the filter was inverted to a clean tube and centrifuged to obtain the protein fraction. The radioactivity in Becquerel from protein fraction ( $A_{\text{protein}}$ ), filtrate and filter unit were measured by gamma counter (Wizard, PerkinElmer), and gave the sum of these radioactivities as  $A_{\text{total}}$ . The free fraction of (R)-[<sup>11</sup>C]YH132 in plasma was calculated using equation 1.

$$f_u = 1 - \frac{A_{\text{protein}}}{A_{\text{total}}} \quad (1)$$

### In vivo PET scans

Dynamic PET scans were carried out in mice immobilized by isoflurane inhalation inside PET/CT scanner (Super Argus, Sedecal, Madrid, Spain). The tracer (8.67–12.99 MBq, 0.12–1.26 nmol/kg) was injected intravenously 1 min before the data acquisition, which lasted for 60 min. The respiratory rate and body temperature of the animal during the scan were monitored as described elsewhere.<sup>[35]</sup> For blocking studies, a 0.008 mg/kg or 0.045 mg/kg dose of MAGLi 432 was injected to the animal shortly before administration of the radiotracer.

### Data analysis and statistical analysis

Data analysis of *in vitro* autoradiograms was performed using AIDA 4.50.010 software (Raytest Isotopenmessgeräte GmbH, Straubenhardt, Germany). Semiquantification of radioactive signals was carried out based on the density of photostimulated luminescence (PSL) in the whole brain area (pixel) expressed PSL per pixel. Regional information for semiquantification is provided in supporting information (Table S1–2). The reconstruction of dynamic PET data was accomplished in a user-defined time frames (3×60, 2×120, 1×210, 1×300, 1×450, 1×750 and 1×900 s) with a voxel size of 0.3875×0.3875×0.775 mm<sup>3</sup>. The ROI template was previously generated by drawing different brain regions on mouse T2-weighted (W. Schiffer) MR images provided by PMOD v4.002 (PMOD Technologies, Zurich, Switzerland). After spatial transformation of a predetermined ROI template to the imaging data, registration parameters were applied to ROIs to individual PET scans. The tissue or region activity was expressed as standardized uptake value (SUV)

decay-corrected to image-derived radioactivity per cm<sup>3</sup> to injected dose per gram of body. The statistical significance of the data was evaluated in Microsoft Excel 2013 with student's *t* test (two-tailed, homoscedastic).

### Acknowledgements

We thank Isabelle Kaufmann (Roche Innovation Center Basel) and Eric Bald (Roche Innovation Center Basel) for their kind technical assistance, and thank Bruno Mancosu (ETH Zurich) for supporting cyclotron and module. Y. He is particularly grateful for the generous financial support from China Scholarship Council (CSC201706040066). This research work was financially supported by the Swiss National Science Foundation (SNSF Grant 205321\_192409/1 to L. Mu). Open Access funding provided by Eidgenössische Technische Hochschule Zürich.

### Conflict of Interests

The authors declare no conflict of interest.

### Data Availability Statement

The data that support the findings of this study are available on request from the corresponding author. The data are not publicly available due to privacy or ethical restrictions.

**Keywords:** monoacylglycerol lipase · *in vitro* autoradiography · PET imaging

- [1] O. Aizpurua-Olaizola, I. Elezgarai, I. Rico-Barrio, I. Zarandona, N. Etxebarria, A. Usobiaga, *Drug Discovery Today* **2017**, *22* (1), 105–110.
- [2] M. Maccarrone, V. Marzo, J. Gertsch, U. Grether, A. C. Howlett, T. Hua, A. Makriyannis, D. Piomelli, N. Ueda, M. van der Stelt, *Pharmacol Rev.* **2023**, *75*, 885–958.
- [3] J. R. Savinainen, S. M. Saario, J. T. Laitinen, *Acta Physiol.* **2012**, *204* (2), 267–276.
- [4] J. L. Blankman, G. M. Simon, B. F. Cravatt, *Chem. Biol.* **2007**, *14* (12), 1347–1356.
- [5] D. K. Nomura, B. E. Morrison, J. L. Blankman, J. Z. Long, S. G. Kinsey, M. C. G. Marcondes, A. M. Ward, Y. K. Hahn, A. H. Lichtman, B. Conti, et al., *Science* **2011**, *334* (6057), 809–813.
- [6] R. M. Ransohoff, *Science* **2016**, *353* (6301), 777–783.
- [7] J. R. Piro, D. I. Benjamin, J. M. Duerr, Y. Q. Pi, C. Gonzales, K. M. Wood, J. W. Schwartz, D. K. Nomura, T. A. Samad, *Cell Rep.* **2012**, *1* (6), 617–623.
- [8] L. Cristino, T. Bisogno, V. Di Marzo, *Nat. Rev. Neurol.* **2020**, *16* (1), 9–29.
- [9] A. Gil-Ordóñez, M. Martín-Fontecha, S. Ortega-Gutiérrez, M. L. López-Rodríguez, *Biochem. Pharmacol.* **2018**, *157*, 18–32.
- [10] N. L. Grimsey, J. R. Savinainen, B. Attili, M. Ahamed, *Drug Discovery Today* **2020**, *25* (2), 330–343.
- [11] R. Chen, J. Zhang, Y. Wu, D. Wang, G. Feng, Y.-P. P. Tang, Z. Teng, C. Chen, *Cell Rep.* **2012**, *2* (5), 1329–1339.
- [12] N. Pasquarelli, C. Porazik, H. Bayer, E. Buck, S. Schildknecht, P. Weydt, A. Witting, B. Feger, *Neurochem. Int.* **2017**, *110*, 14–24.
- [13] C. Syal, J. Kosaraju, L. Hamilton, A. Aumont, A. Chu, S. N. Sarma, J. Thomas, M. Seegobin, F. Jeffrey Dilworth, L. He, et al., *Theranostics* **2020**, *10* (14), 6337–6360.
- [14] A. H. Jacobs, H. Li, A. Winkeler, R. Hilker, C. Knoess, A. Rüger, N. Galldiks, B. Schaller, J. Sobesky, L. Krach, et al., *Eur. J. Nucl. Med. Mol. Imaging* **2003**, *30* (7), 1051–1065.

- [15] D. Bertoglio, L. Kosten, J. Verhaeghe, D. Thomae, L. Wyffels, S. Stroobants, J. Wityak, C. Dominguez, L. Mrzljak, S. Staelens, *J. Nucl. Med.* **2018**, *59* (11), 1722–1727.
- [16] Y. He, M. Schild, U. Grether, J. Benz, L. Leibrock, D. Heer, A. Topp, L. Collin, B. Kuhn, M. Wittwer, et al., *J. Med. Chem.* **2022**, *65* (3), 2191–2207.
- [17] A. Kemble, B. Hornsperger, I. Ruf, H. Richter, J. Benz, B. Kuhn, D. Heer, M. Wittwer, B. Engelhardt, U. Grether, L. Collin, *PLoS ONE* **2022**, *17* (9), e0268590.
- [18] Y. Hattori, K. Aoyama, J. Maeda, N. Arimura, Y. Takahashi, M. Sasaki, M. Fujinaga, C. Seki, Y. Nagai, K. Kawamura, et al., *J. Med. Chem.* **2019**, *62* (5), 2362–2375.
- [19] T. P. Dinh, D. Carpenter, F. M. Leslie, T. F. Freund, I. Katona, S. L. Sensi, S. Kathuria, D. Piomelli, *Proc. Nat. Acad. Sci.* **2002**, *99* (16), 10819–10824.
- [20] C. Wang, M. S. Placzek, G. C. Van De Bittner, F. A. Schroeder, J. M. Hooker, *ACS Chem. Neurosci.* **2016**, *7* (4), 484–489.
- [21] L. Zhang, C. R. Butler, K. P. Maresca, A. Takano, S. Nag, Z. Jia, R. Arakawa, J. R. Piro, T. Samad, D. L. Smith, et al., *J. Med. Chem.* **2019**, *62* (18), 8532–8543.
- [22] Atlas.brain-map.org., A. R. A. – M. B. [brain atlas]. Available from Atlas-Brain-Map.Org.
- [23] M. Honer, L. Gobbi, L. Martarello, R. A. Comley, *Drug Discovery Today* **2014**, *19* (12), 1936–1944.
- [24] L. Zhang, A. Villalobos, E. M. Beck, T. Bocan, T. A. Chappie, L. Chen, S. Grimwood, S. D. Heck, C. J. Helal, X. Hou, et al., *J. Med. Chem.* **2013**, *56* (11), 4568–4579.
- [25] A. Haider, L. Gobbi, J. Kretz, C. Ullmer, A. Brink, M. Honer, T. J. Woltering, D. Muri, H. Iding, M. Bürkler, et al., *J. Med. Chem.* **2020**, *63* (18), 10287–10306.
- [26] A. Haider, L. Wang, L. Gobbi, Y. Li, A. Chaudhary, X. Zhou, J. Chen, C. Zhao, J. Rong, Z. Xiao, et al., *ACS Chem. Neurosci.* **2023**, *14* (20), 3752–3760.
- [27] Y. He, L. C. Gobbi, A. M. Herde, D. Rombach, M. Ritter, B. Kuhn, M. B. Wittwer, D. Heer, B. Hornsperger, C. Bell, et al., *Nucl. Med. Biol.* **2022**, *108*, 24–32.
- [28] Y. He, U. Grether, M. F. Taddio, C. Meier, C. Keller, M. R. Edelmann, M. Honer, S. Huber, M. B. Wittwer, D. Heer, et al., *Eur. J. Med. Chem.* **2022**, *243*, 114750.
- [29] G. Boscutti, M. Huiban, J. Passchier, *Drug Discovery Today Technol.* **2017**, *25*, 3–10.
- [30] S. Jiang, S. Berger, Y. Hu, D. Bartsch, Y. Tian, *Front. Neurol. Neurosci.* **2020**, *14* (April), 1–11.
- [31] N. Takahashi, L. L. Miner, I. Sora, H. Ujike, R. S. Revay, V. Kostic, V. Jackson-Lewis, S. Przedborski, G. R. Uhl, *Proc. Natl. Acad. Sci. USA* **1997**, *94* (18), 9938–9943.
- [32] T. N. Taylor, W. M. Caudle, G. W. Miller, *Parkinsons. Dis.* **2011**, *2011*.
- [33] R. Slavik, U. Grether, A. Müller Herde, L. Gobbi, J. Fingerle, C. Ullmer, S. D. Krämer, R. Schibli, L. Mu, S. M. Ametamey, *J. Med. Chem.* **2015**, *58* (10), 4266–4277.
- [34] M. F. Taddio, L. Mu, C. A. Castro Jaramillo, T. Bollmann, D. M. Schmid, L. P. Muskalla, T. Gruene, A. Chiotellis, S. M. Ametamey, R. Schibli, et al., *J. Med. Chem.* **2019**, *62* (17), 8090–8100.
- [35] A. Haider, J. Kretz, L. Gobbi, H. Ahmed, K. Atz, M. Bürkler, C. Bartelmus, J. Fingerle, W. Guba, C. Ullmer, et al., *J. Med. Chem.* **2019**, *62* (24), 11165–11181.

Manuscript received: December 4, 2023

Revised manuscript received: January 12, 2024

Version of record online: March 5, 2024